Microbe-metabolite associations linked to the rebounding murine gut microbiome post-colonization with vancomycin resistant *Enterococcus faecium*

Andre Mu[a,b,c,#], Glen P. Carter[a], Lucy Li[a], Nicole S. Isles[a,c], Alison F. Vrbanac[d,e], James T. Morton[f], Alan K. Jarmusch[g,h], David P. De Souza[i], Vinod K. Narayana[i], Komal Kanojia[j], Brunda Nijagal[k], Malcolm J. McConville[i,k], Rob Knight[d,e,l,m], Benjamin P. Howden[a,b,c] and Timothy P. Stinear[a,b]

[a]Department of Microbiology and Immunology at the Peter Doherty Institute for Infection and Immunity, University of Melbourne, Australia

[b]Doherty Applied Microbial Genomics, Department of Microbiology and Immunology at the Peter Doherty Institute for Infection and Immunity, Australia

[c]Microbiological Diagnostic Unit Public Health Laboratory, at the Peter Doherty Institute for Infection and Immunity, University of Melbourne, Australia

[d]Department of Pediatrics, University of California San Diego, USA

[e]Department of Computer Science & Engineering, University of California San Diego, USA

[f]Flatiron Institute, Centre for Computational Biology, USA

[g]Skaggs School of Pharmacy and Pharmaceutical Sciences, University of California San Diego, USA

[h]Collaborative Mass Spectrometry Innovation Center, Skaggs School of Pharmacy and Pharmaceutical Sciences, University of California San Diego, USA

[i]Metabolomics Australia, Bio21 Institute of Molecular Science and Biotechnology, University of Melbourne, Australia

[j]Centre for Biostatistics and Clinical Trials, Peter MacCallum Cancer Centre, Victoria, Australia

26 [k]Department of Biochemistry and Molecular Biology, University of Melbourne, Australia

27 [l]Department of Bioengineering, University of California San Diego, USA

28 [m]Center for Microbiome Innovation, University of California San Diego, USA

29

30 Running head: Gut microbiome and colonization with VRE

31 #Address correspondence to Dr. Andre Mu, andre.mu@unimelb.edu.au

32 B.P.H and T.P.S contributed equally to this work.

33 Word count: 2,850

34

35 mSystems Host-Microbe Biology

36

37 **Keywords**

38 Microbiome, multi-omics, metagenomics, metabolomics, gut microbiome, vancomycin

39 resistant *Enterococci*, colonization, antimicrobial resistance

40

41 **Abstract**

42 Vancomycin resistant *Enterococcus faecium* (VREfm) is an emerging antibiotic resistant

43 pathogen. Strain-level investigations are beginning to reveal the molecular mechanisms used

44 by VREfm to colonize regions of the human bowel. However, the role of commensal bacteria

45 during VREfm colonization, in particular following antibiotic treatment, remains largely

46 unknown. We employed amplicon 16S rRNA gene sequencing and metabolomics in a murine

47 model system to try and investigate functional roles of the gut microbiome during VREfm

48 colonization. First-order taxonomic shifts between Bacteroidetes and Tenerricutes within the

49 gut microbial community composition were detected both in response to pretreatment using

50 ceftriaxone, and to subsequent VREfm challenge. Using neural networking approaches to find

co-occurrence profiles of bacteria and metabolites, we detected key metabolome features associated with butyric acid during and after VREfm colonization. These metabolite features were associated with *Bacteroides*, indicative of a transition towards a pre-antibiotic naïve microbiome. This study shows the impacts of antibiotics on the gut ecosystem, and the progression of the microbiome in response to colonisation with VREfm. Our results offer insights towards identifying potential non-antibiotic alternatives to eliminate VREfm through metabolic re-engineering to preferentially select for *Bacteroides*.

Importance

This study demonstrates the importance and power of linking bacterial composition profiling with metabolomics to find the interactions between commensal gut bacteria and a specific pathogen. Knowledge from this research will inform gut microbiome engineering strategies, with the aim of translating observations from animal models to human-relevant therapeutic applications.

Introduction

Vancomycin-resistant *Enterococcus faecium* (VREfm) is a significant healthcare-associated pathogen. VREfm infections can be difficult to treat due to their intrinsic and acquired resistance to nearly all classes of antibiotics (1). The World Health Organisation categorizes VREfm as a "High Priority" bacterial pathogen, advocating research to stop the global increase in antibiotic resistance (2). Recent studies highlight the importance of the gut microbiota in modulating the growth and virulence of VRE*fm* in the gastrointestinal ecosystem. For instance, the depletion of normal gut flora using antibiotics exacerbates the severity of VREfm infection (3), whereas transplant of commensal species including a consortium of *Clostridium bolteae*, *Blautia producta*, *Blautia sartorii*, and *Parabacteroides distasonis* (4, 5) can drive established

76 VREfm colonisation to below levels of culture detection. Specifically, *B. producta* – a
77 colonizer of the colon – reduces VREfm growth *in vivo* by secreting a lantibiotic (6). These
78 observations raise the intriguing possibility that metabolic traits act in concert between
79 pathogen and select gut commensals to confer mutual benefits during pathogen persistence.
80 These findings also highlight the greater risk posed to immunocompromised patients when
81 colonized with VREfm. For instance, allogeneic hematopoietic cell transplantation patients
82 have gastrointestinal tracts that are dominated by VREfm as a result of losing a large portion
83 of the intestinal commensal microbiota upon receiving broad-spectrum antibiotics as pre-
84 treatment(7). Hildebrand et al., (2018) discovered long-term ecological impacts to the gut
85 microbiome, with strong bacterial species turnover, after ceftriaxone treatment in humans (8).
86 Further, mice receiving broad spectrum antibiotics (combination of metronidazole, neomycin,
87 and vancomycin) showed markedly increased VREfm colonization of the caecum and colon.
88 The compromised intestinal innate immune defenses in these animals allowed proliferation of
89 VREfm caused by the antibiotic exposure and subsequently reduced the expression of
90 antimicrobial molecules produced by bacteria in the intestinal mucosa (9).

91 The problem with VREfm is further complicated by the fact that *Enterococci* are
92 members of the gastrointestinal tract microbiota; a key reservoir of antimicrobial resistance
93 (AMR) genes, and potentially facilitating gene transfer within the gut microbiome (10). For
94 example, the *vanB* resistance gene was detected in human faecal specimens that did not contain
95 culturable VRE; and instead, demonstrated that isolates carrying the resistance transposon are
96 anaerobic commensal bacteria, *Eggerthella lenta* and *Clostridium innocuum*(11). Colonisation
97 of, and persistence in, the gastrointestinal tract therefore presents as a key mechanism for *de*
98 *novo* VRE and may lead to severe invasive disease.
99

100 This current study aimed to understand the impact of antibiotics on the murine gut microbiota,
101 and the subsequent colonisation pattern of VREfm. To this extent, we designed a murine model
102 time-series study that consisted of two main perturbative phases: (1) antibiotic pre-treatment
103 with ceftriaxone, and (2) VREfm challenge. Our 16S rRNA gene profiling analyses
104 highlighted a first-order shift in bacterial biodiversity composition across time, a second-order
105 clustering of samples associated with the experimental phases, and the transition of the post-
106 VREfm colonisation gut microbiota and its metabolome towards resembling an asymptomatic
107 carriage-like microbiome phenotype. This research provides support for engineering the
108 metabolic potential of the gut microbiome using, for example, prebiotics as a non-antibiotic
109 alternative for treating multi-drug resistant bacterial infections.
110
111 **Results**
112 *Experimental design.*
113 The following experimental design was developed to address the hypothesis that there are
114 specific murine gut microbiome factors that facilitates VREfm colonization; three groups of
115 three C57BL/6 mice (co-caged wildtype males) were monitored, and fecal samples collected,
116 over a fourteen-day period with two intervention time-points; including (1) ceftriaxone
117 treatment administered at 0.5g/L in drinking water across a two-day period, and (2)
118 colonisation (via oral-gavage) with 1 x 10^6 VREfm ST796 per mice post-antibiotic treatment
119 at a single timepoint. Mice were housed in groups of five and samples collected from the same
120 three mice to represent technical replicates per cage; herein, each group of co-housed mice will
121 be referred to as Group A, Group B, and Group C. The remaining two mice per group were
122 reserved for microbiological assays. Table 1 highlights samples and datasets collected.
123

124 *Amplicon 16S rRNA gene sequencing revealed first order shifts in bacterial community*
125 *composition.*
126 Amplicon 16S rRNA gene sequencing was performed to capture the bacterial community
127 composition in an effort to track changes in response to antibiotic pre-treatment and VREfm
128 colonization. Bacterial community profiles were assessed in fecal samples from nine mice
129 before, during and after the two interventions (Table 1). A total of 71.32% of reads (10,519,073
130 reads) passed quality control, with 321,955 reads on average per sample and a total of 3574
131 exact variant sequence types (i.e., features), with an average of 118 features per sample, and
132 an upper bound of 246 features (when rarefied to 20,000 reads). Alpha rarefaction analysis
133 demonstrated sufficient sequencing depth to capture microbial diversity to saturation
134 (Supplementary Figure 1).
135 The biodiversity profiles of each sample were compared and showed that key sOTUs
136 were differentially abundant throughout the course of the experiment (Figure 1). There was a
137 shift in the dominance of Bacteroidia (Bacteroidetes; light green coloured bars) during the
138 naïve phase of the experiment to Mollicutes (Tenericutes; fuschia coloured bars) in response
139 to ceftriaxone treatment, with a return to the predominance of Bacteroidia during the late-phase
140 of the experiment, post-VREfm colonisation (i.e., days 12 – 14). Of note is the predominance
141 of Lactobacillales in Mouse 1 – 3 from Group A (Figure 1).
142
143 *The murine gut microbiota responds to antibiotics and microbial community richness begins*
144 *to rebound three-days post-VRE colonisation.*
145 Principal coordinate analysis (PCoA) of the unweighted UniFrac (12) distances was used to
146 assess clustering of fecal samples based on bacterial composition. This assessment showed that
147 the fecal microbiota from samples collected from each phase clustered together but were
148 clearly separated between phases; after exposure to ceftriaxone, and challenge with VREfm

149 post-antibiotic treatment (Figure 2A). Permutation-based statistical testing demonstrates the
150 groups are significantly different from one another (Supplementary Figure 2). Temporal
151 tracking of the changing microbiomes against each mouse on the PCoA sample-space
152 demonstrated a clear, unidirectional trajectory that followed the chronology of the experiment
153 (animation as a supplementary file). Procrustes analyses of weighted and unweighted UniFrac
154 distances showed that the same general patterns on the sample space were preserved, meaning
155 that there is congruency in global spatial patterns between qualitative and quantitative measures
156 of community dissimilarity (Supplementary Figure 3).

157 Analysis of community diversity (Faith's Phylogenetic Diversity Index) revealed a
158 stable and rich microbial community during the naïve phase preceding a sharp decrease
159 following antibiotic treatment, and a further decrease immediately following VREfm
160 colonisation (Figure 2B). Of note is the responsiveness of the microbiota (within 24 h) to the
161 removal of antibiotics at the end of day 7. Community richness began to rebound at
162 approximately three-days post-VREfm colonisation (i.e., day 12), with Group A demonstrating
163 a faster rate of rebound compared to Group B and C. Calculating the distances of dissimilarity
164 (unweighted UniFrac distances) of each mouse microbiota timepoint relative to Day 0 (a proxy
165 for the naive bacterial community phenotype) revealed a small dissimilarity distance for
166 samples collected during the naïve phase, and an increasing dissimilarity distance following
167 antibiotic treatment (day 6) and VREfm colonisation (day 9; Figure 2C). There was a
168 downward trajectory in distance scores at three-days post-VREfm colonisation (i.e., day 12);
169 Group A followed a sharper return to a microbiota resembling day 0. These observations
170 suggest that mice were transitioning towards a persistent carrier-like state, and that the
171 rebounding community richness towards levels representative of the naïve phase was by a
172 microbial community structure that resembled the naïve phase. Additional studies where the
173 time-frame of post-VREfm challenge extends beyond one-week of monitoring are needed to

174 understand if the perturbed microbiome will return to resemble an absolute naïve state or arrive
175 at a new, altered state.
176
177 *Multinomial regression identifies sOTUs most positively associated with VREfm colonisation.*
178 Multinomial regression using *Songbird* was employed to identify sOTUs that were most
179 positively, and negatively, associated with the post-VREfm colonisation phase (Figure 3). The
180 five most positively associated sOTUs were *Enterococcus*, *Bacteroides*, *Erysipelotrichaceae*,
181 *Catabacter*, and *Lachnospiraceae*; while the five most negatively associated were
182 *Clostridiales*, *Adlercreutzia*, *Mollicutes*, *Peptostreptococcaceae*, and *Clostridiales*. Temporal
183 tracking of exact sequence variants (ESV) demonstrated that the ESV feature classified as
184 *Enterococcus* - and identified as the most positively associated with the post-VREfm
185 colonisation phase - was most abundant on days of challenge; confirming that this ESV likely
186 was the ST796 VREfm colonization challenge organisms (Figure 3). There were a further eight
187 ESV features classified as *Enterococcus*, however, they were absent during the days
188 representing VREfm colonisation, and lacked positive associations with the post-VREfm
189 colonisation phase, suggesting that these features represent murine gut commensal
190 Enterococci.
191
192 *Molecular networking identifies differential metabolome profiles.*
193 Duplicate fecal samples from key timepoints throughout the experiment (i.e., days 0, 5, 6, 7, 8,
194 9, and 14) were analysed by data dependent tandem mass spectrometry (MS/MS) performed
195 on a liquid-chromatography quadrupole time-of-flight (LC-QTOF) to monitor changes in the
196 murine gut metabolome (Table 1). Polar metabolite analysis was preferenced in an effort to
197 broadly capture primary metabolites which play a key role in "metabolic hand-offs" that define
198 interspecies interactions. Analysis of the global metabolome profile of each sample was

199 measured based on their overlapping molecules, and a PCoA plot using a binary Jaccard
200 distance metric through the Global Natural Products Social Molecular Networking (GNPS)
201 platform (13). A separation of metabolite profiles along PCoA1 was observed (57.34% Figure
202 4A). Metabolomes from the naïve, and late-VREfm colonisation phase tended to cluster
203 together, while samples from the post-antibiotic phases including the early-VREfm
204 colonisation phase clustered together. Supporting pairwise PERMANOVA testing
205 (Supplementary Figure 4) highlights naïve and early-VRE samples are significantly different,
206 while late-VRE has a lower distance to naïve compared to antibiotic treated, antibiotic wean
207 and early-VRE samples.
208 Random forest analysis of spectra profiles from LC-MS/MS was used to predict experimental
209 phase and rank the importance of metabolite association with each experimental phase. The
210 top metabolite features for each experimental phase are highlighted in Figure 4B. Unique
211 profiles of metabolite features were observed for each phase of the experiment. Importantly,
212 the late-VREfm colonisation phase captures an unknown metabolite (feature 6325) with a
213 mass-to-charge ratio (m/z) of 173.067 and retention time (RT) of 18.392; this metabolite is
214 exclusively present during what represents the *transition* towards resembling the naïve
215 microbiome. Manual curation of feature 6325 in positive ion mode predicts a molecular
216 formula $C_5H_8N_4O_3$ with ≥ 10 ppm in mass error. The major peaks in the MS/MS spectrum for
217 feature 6325 are: 173.07 (precursor ion, [M+H]+ assumed), 155.06 (precursor ion, 18(H_2O),
218 113.05 (155.06 product ion, 42.01 (likely C_2H_2O), 43.03 ([C_2H_2O+H] + product ion further
219 supporting neutral loss of C_2H_2O); given the summation of results, the chemical structure of
220 feature 6325 is likely to contain a N-acetylated hydroxyl group. Peak quantification values
221 indicate its presence during the late phase of VRE colonisation (Figure 4C). Further manual
222 curation of MS/MS data identified ceftriaxone as feature 3901 with an m/z = 555.0537 and RT
223 = 13.30, and mostly abundant during days of antibiotic exposure (Figure 4D).

224

225 *Bacteroidales-associated metabolites implicated in late-phase post-VREfm colonisation.*

226 A distinct profile shift in microbe and metabolite abundances (as calculated by multinomial
227 regression) was observed, particularly during late-phase VREfm colonisation (Supplementary
228 Figure 6). Shallow neural networking analysis with *mmvec* was used to predict microbe-
229 metabolite interactions through their co-occurrence probabilities (Figure 5). Sequential biplots
230 captured the shift in experimental phases and highlighted the co-occurrences of microbiota and
231 metabolomic datasets (Fig. 5A,B,C). There was a strong *Enterococcus* effect as indicated by
232 the magnitude of the corresponding arrow, and the rebounding species during the late-phase
233 VREfm colonisation are predominantly *Bacteroidales* sOTUs (Figure 5C) with co-occurring
234 metabolite features m/z 173.067 RT 18.392, and m/z 167.083 RT 25.277. Metabolite feature
235 mz 245.055 RT 7.945 was ranked as being highly associated with the post-VRE colonisation
236 phase. These results integrate microbial and metabolite datasets to reveal which microbes may
237 be responsible for detected metabolites. In this instance, the metabolite present during the phase
238 representing a *transition* towards a microbiome approximating the naïve state (feature 6325
239 m/z 173.067 and RT 18.392; Figure 4B) is linked with *Bacteroidales* (Figure 5A).

240

241 **Discussion**

242 In this study of the murine gut ecosystem, we employed a mouse model of gastrointestinal tract
243 colonisation that replicates the shift in bacterial composition when patients enter the healthcare
244 system, develop an imbalance in microbiome as a result of pre-treatment (e.g., antibiotic
245 treatment), and are subsequently colonised with a hospital superbug (14). The resolution of
246 current studies describes a consortium of commensal microbes that can, for example, reduce
247 the magnitude of VREfm colonisation (4, 6); however, understanding the key metabolic shifts
248 relative to the gut microbiota remains challenging (15). Here, we employed amplicon 16S

249 rRNA gene sequencing and high-resolution mass spectrometry metabolomics in an effort
250 towards determining microbiota-metabolome interactions during VREfm colonisation. We
251 demonstrated clear changes in the gut microbiome in response to ceftriaxone and VREfm
252 challenge.
253
254 Conceptual and statistical advances in analysis of amplicon 16S rRNA gene data (16, 17)
255 whereby OTUs are clustered at a 99% nucleotide similarity threshold allows for the
256 identification of exact sequence variants (ESV). Query against an error-corrected database (17)
257 can detect multiple ESVs that may be classified to the same taxonomic rank. For example, our
258 analyses identified multiple ESVs classified as *Enterococci*; however, when the relative
259 abundances were tracked across the chronology of the experiment, only one *Enterococci*-ESV
260 was dominant in relative abundances and most positively associated with the days of post-
261 VREfm challenge (Figure 3). This highlights the resolving power to differentiate between
262 commensal and pathogenic strains of *Enterococci* when the composition of the microbial
263 community is considered. The fact that this was achievable at the level of amplicon 16S rRNA
264 gene sequencing alludes to the possibility of implementing microbiota screenings as routine
265 diagnostics for patients entering healthcare systems. Further, first-order level shifts in
266 microbial community composition was observed in response to ceftriaxone and subsequent
267 VREfm challenge (Figure 1). At three days post-VREfm colonisation (i.e., day 12), the
268 microbiome richness begins to rebound; suggesting that mice are transitioning towards a
269 persistent carrier-like state. Interestingly, Group A cohort exhibited a faster rate of rebound
270 that may be facilitated by their initially higher microbial community richness and
271 predominance of Lactobacillales during day of VREfm challenge (Figure 2B); this observation
272 supports the need to prescreen "baseline" microbiota profiles of patients upon admission into
273 hospital for the reason that it is not necessarily which microbial populations are removed post-

274 perturbation (e.g., antibiotic pre-treatment) but instead, which populations persist that drives
275 the responding phenotype. We can begin to assess patients from across different wards (e.g.,
276 intensive care unit, oncology, neurology, and healthy cohorts), and build a database of
277 microbiome profiles that can be used as biomarkers to predict: (1) the susceptibility of patients
278 to develop persistent bacterial colonisation, and (2) propensity to clear the pathogen once
279 colonized. The clinical implication is that new patients are screened and identified (via beta-
280 diversity meta-analyses) by these biomarkers and placed in bedding cohorts accordingly;
281 thereby improving infectious disease management and isolation precautions within health-care
282 associated ecosystems.
283
284 The shortlist of microbes ranked as most negatively associated with the colonisation phase
285 (*Clostridiales*, *Adlercreutzia*, *Mollicutes*, *Peptostreptococcaceae*, and *Clostridiales*; Figure 3)
286 are hypothesized to play a role in maintaining the health of the animals. Indeed, amongst the
287 microbes identified, are known short chain fatty acid (e.g., butyric acid) producers (18, 19) that
288 supports, and expands upon those previously identified by Caballero et al., (2017). Further, the
289 use of Deblur to identify ESVs facilitates the temporal tracking of their relative abundances to
290 inform selection of primary fecal samples that will provide the best probability (i.e., highest
291 relative abundance) of culturing target taxa for downstream screening of probiotic potential.
292 However, translating animal-derived observations from experimental animal models to human
293 clinical situations remains challenging; particularly where the key microbes are rodent-
294 specific. One solution may be to integrate metabolomics to reveal shared metabolic capacity
295 amongst taxonomically divergent microbes. Our supervised classifying approaches suggests
296 an altered metabolome composition during the late-phase of VREfm challenge that may
297 facilitate the apparent "suppression" of VREfm to levels below the limit-of-detection by
298 culture. Despite the caveat of poor resolution in current databases to link metabolite features

299 to associated chemical structures, microbe-metabolite vector analysis linked metabolite feature
300 6325 (m/z = 173.067 RT = 18.392) to *Bacteroides* (Figure 5). Our efforts towards manually
301 identifying feature 6325 suggests a chemical formula of $C_5H_8N_4O_3$ and a structure likely to
302 contain a N-acetylated hydroxyl group; a putative annotation (through *pubchem* search) is 3-
303 hydroxy-4-(nitrosocyanamido) butyramide. Butyramide is the amide group of butyric acid, a
304 short-chain fatty acid that has been shown to play a key role in colonisation resistance against
305 intestinal pathogens (20–23). Further research to comprehensively characterize interactions
306 between microbe and metabolites will be critical to address the gaps in our understanding of
307 the biochemical parameters that define interspecies microbiome interactions during antibiotic
308 pre-treatment and persistent infections.
309
310 The resolution of our results provides the basis in which to begin to identify non-antibiotic
311 alternatives to engineer the gut microbiome through prebiotic interventions (e.g., butyric acid),
312 and translating animal studies to human-relevant therapeutic applications by delineating
313 taxonomically diverse microbes with shared metabolic capacity. Here, achieving integrative
314 omics to link microbe-metabolite associations, our findings adds support to the incorporation
315 a microbiome profiling approaches into routine clinical microbiology, particularly in the
316 context of monitoring the impacts of antibiotic use.
317
318 **Methods**
319 *Mouse gastrointestinal colonization model.*
320 Six-week old wild type C57BL/6 male mice were used to establish an animal model of
321 gastrointestinal colonisation with VREfm. Mice were co-housed, they have free access to food
322 (ordinary chow) and water and have environmental enrichment (e.g., fun tunnels, chew blocks,
323 and tissue paper). The light/dark cycle was 12 h light/ 12 h dark, and cages were changed

324 weekly. Mice were pretreated with 0.5 g/L ceftriaxone in drinking water for two-days followed
325 by an antibiotic wean period of 24 h. Mice were then challenged with 1 x 10^6 cfu VREfm
326 ST796.
327
328 *Genomic DNA extraction and sequencing.*
329 Whole community gDNA was extracted from mouse faecal samples using the Qiagen
330 PowerSoil DNA Extraction Kit (formerly MoBio) following the manufacturer's protocol. A
331 preprocessing step of mechanical lysis was incorporated using a Bertin Technologies
332 Precellysis 24 machine for one round of a 40 second-cycle at 6000 rpm. The V4 region of the
333 bacterial 16S rRNA gene was amplified using small subunit 515 forward Golay-barcoded, and
334 SSU806 reverse primers following the Earth Microbiome Project protocol
335 (www.earthmicrobiome.org;(24)), and sequenced using the Illumina MiSeq platform (V2, 300
336 cycles; Illumina Inc., San Diego, USA). Sample metadata and sequence data for the current
337 study were deposited into *QIITA* (25) - an open-source management platform for research
338 studies with multiple 'omic datasets - under the project title *Mouse-hospital VRE colonization*
339 *with ceftriaxone treatment* (Study ID 11737). Further, primary derived data (e.g., BIOM tables)
340 used to produce results can be found within QIITA study ID 11737. Raw sequence data are
341 also available through the NCBI SRA, BioProject number: PRJNA590613
342
343 *Amplicon 16S rRNA gene profiling analyses.*
344 Sequence data were processed within the *QIITA* (v0.1.0) framework for quality control (split
345 libraries v. q2.1.9.1), demultiplexing, trimming sequence reads to a length of 150 nt, and
346 picking sub-operational taxonomic units (sOTUs) using *Deblur* (v1.1.0) to resolve single-
347 nucleotide community sequencing patterns (*i.e.* feature identification of sOTUs;(17)). The
348 output BIOM files were further processed using *QIIME2* (v2019.7) for downstream statistical

349 analyses(26). Alpha rarefaction curves were generated to determine if each sample had been
350 sequenced to saturation; the feature table was subsequently rarefied to 20,000 reads per sample.
351 Taxonomy was assigned using the *sklearn* classifier (27) and *Greengenes 13.8 99% OTUs from*
352 *515F/806R region of sequences* classifier available from https://docs.qiime2.org/2018.4/data-
353 resources/. Furthermore, relative abundances of each taxa were visualized as bar plots using
354 the QIIME2 *taxa* plugin. A phylogenetic tree was constructed using fragment-insertion
355 (*QIIME fragment-insertion sepp;* (28)) to guide phylogenetic-aware statistical analyses
356 generated using the *QIIME2* plugin, *q2-diversity core-metrics-phylogenetic*; key metrics
357 computed by default include both alpha-diversity (e.g., Shannon's diversity index, Faith's
358 phylogenetic diversity, and Evenness), and beta-diversity (e.g., Bray-Curtis distance, and
359 unweighted UniFrac distances) metrics. The unweighted UniFrac distance matrix (12) was
360 used to compute first distances and calculate distances relative to Day 0 as baseline between
361 sequential states (*QIIIME longitudinal first-distances*); *ggplot2* (R v3.6.0,
362 https://ggplot2.tidyverse.org) was used to visualize the distance scores as line plots. *Emperor*
363 was used to visualize principal coordinate analysis plots of unweighted UniFrac distances.
364 Permutation-based statistical testing (PERMANOVA) on unweighted UniFrac distances was
365 used to determine if samples grouped by *phase of experiment* were significantly different from
366 one another (*q2-beta-group-signifcance*). *Songbird* (https://github.com/mortonjt/songbird)
367 was employed to determine the importance (*i.e.,* fold change) of each sOTU in relation to a
368 given metadata variable (e.g., VREfm-colonisation). Microbial features from all samples were
369 split into training and test sets for supervised learning classifier analyses; 20% of input samples
370 were allocated to train the Random Forest Classifier within QIIME2, the estimator method
371 used for sample prediction. The different experimental phases were the response variables,
372 while the 16S rRNA gene data were the features.
373

374 *Metabolite extraction and liquid chromatography tandem mass-spectrometry analysis.*

375 Duplicate fecal samples, as outlined in Table 1, were processed for polar metabolite extraction
376 and analysis (days 0, 5, 6, 7, 8, 9, and 14). Feces were metabolically arrested by immediate
377 collection into dry ice, and stored at -80˚C until further processing. Metabolite extraction from
378 the fecal samples was undertaken by the addition of 500 μL per sample of methanol:water
379 solution (3:1 v/v) containing 2μM ^{13}C-sorbitol and 8μM ^{13}C,^{15}N-valine, and 2μM ^{13}C-leucine
380 as internal standards. Fecal samples were homogenized at 1200 rpm for 30 minutes in a
381 thermomixer maintained at 4°C, and mechanically disrupted and incubated for a further 15
382 minutes in the thermomixer. Samples were randomized for metabolite extraction.

383 Metabolite analysis of the extracted samples, pooled biological quality control (PBQC)
384 samples, and 13 mixtures of authentic standards mixes was performed by liquid
385 chromatography mass spectrometry (LC-MS) using hydrophilic interaction column (ZIC-
386 pHILIC) and high-resolution Agilent 6545 series quadrupole time-of-flight mass spectrometry
387 (QTOF MS) as described previously (29). PCoA of binary-Jaccard distances of test, standard
388 mixes, and PBQC samples are presented in Supplementary Figure 5. Ions were analyzed in
389 positive mode with full scan range of 85 to 1200 m/z and in data-dependent tandem MS mode
390 to facilitate downstream metabolite identification. Mass spectrometry data were deposited into
391 *QIITA* (25) under the project title *Mouse-hospital VRE colonization with ceftriaxone treatment*
392 (Study ID 11737).

393

394 *Metabolomic analyses.*

395 The data-dependent tandem MS data was processed using *MZmine2* (v2.39) (30) to generate
396 tabular matrices of metabolite features (i.e., m/z and retention time). Masses were detected,
397 and chromatograms built using *Peak Detection* methods within *MZmine2.* Chromatograms
398 were deconvoluted, and isotopic peaks grouped; grouped peaks were aligned using *join aligner*.

399 *Peak list rows filter* method was applied to the aligned peaks, and gaps filled using *peak finder*.
400 The following MZmine2 settings were applied for spectral processing; MS1 mass detection:
401 1E3; MS2 mass detection: 1E2; time span: 0.02; minimum height: 3E3; m/z tolerance: 10 ppm;
402 pairing m/z range for MS2: 0.1; RT range for MS2 scan: 2 min; minimum peak height: 7E3;
403 peak duration: 0.02 – 5.00, baseline: 5E3;0.001, or maximum chance: 2; Join Aligner: 75%
404 25% ratio split; intensity tolerance: 10%; and m/z tolerance: 5 ppm. Feature finding produced
405 a data matrix of MS1 features and associated peak areas. Feature-based molecular networking
406 outputs *(quant.csv*) were generated from *MZmine2* using the *export to GNPS* module, which
407 contains MS1 feature information and a corresponding *mgf* file containing MS2 information
408 linked to MS1 features. Metabolomic features were further analysed within the *Global Natural*
409 *Products Social Networking (GNPS* v1.2.5*;* (13)*)* framework (UCSD, CA, USA). Tandem MS
410 data were processed for identification, dereplication and quantification, including spectral
411 library searches. For example, MS2 spectra of the unknown metabolites are compared with a
412 library of MS/MS spectra generated from structurally characterized metabolites. Further
413 information on the GNPS workflow, and molecular networking can be found in Ming *et al.,*
414 2016 (13). Further, manual interpretation – including, for example, determining molecular
415 formula of the chemical in neutral charge structure, determining theoretical monoisotopic
416 mass, and determining likely adduct - of MS/MS data was applied to identify unknown
417 features.
418
419 *Neural networking to predict microbe-metabolite interactions.*
420 Microbiota and metabolome feature tables were analyzed using *MMVEC*
421 ((31)https://github.com/biocore/mmvec) to identify microbe-metabolite interactions through
422 their co-occurrence probabilities as predicted by neural networking. Conditional biplots were
423 generated using *Emperor*. Further, microbe abundances and metabolite log centered abundance

424 heatmaps were generated using primary derived data from multinomial regression analyses
425 using *Songbird* (https://github.com/mortonjt/songbird).
426

427 **Acknowledgements**
428 We thank the team at Metabolomics Australia (Bio21) mass spectrometry services. We thank
429 Dr. Daniel Petras (UCSD) for helpful discussions.
430

431 **Funding**
432 The project was supported by an Endeavour Research Fellowship (Australia Awards) for
433 collaborative research in the Department of Pediatrics at UCSD, CA, USA (ERF PDR
434 6735_2018) (AM). The project was also supported by the National Medical Research Council
435 of Australia, GNT1105525 (TPS) and GNT 1026656 (BPH). The funders had no role in study
436 design, data collection and interpretation, or the decision to submit the work for publication.
437

438 **References**
439 1. Arias CA, Murray BE. 2012. The rise of the *Enterococcus*: beyond vancomycin resistance.
440 Nat Rev Microbiol 10:266–278.

441 2. Panel GPPL. 2017. Global priority list of antibiotic-resistant bacteria to guide research,
442 discovery, and development of new antibiotics. World Health Organization.

443 3. Ubeda C, Taur Y, Jenq RR, Equinda MJ, Son T, Samstein M, Viale A, Socci ND, van den
444 Brink MR, Kamboj M, Pamer EG. 2010. Vancomycin-resistant *Enterococcus* domination of
445 intestinal microbiota is enabled by antibiotic treatment in mice and precedes bloodstream
446 invasion in humans. J Clin Invest 120:4332–4341.

447 4. Caballero S, Kim S, Carter RA, Leiner IM, Sušac B, Miller L, Kim GJ, Ling L, Pamer EG.
448 2017. Cooperating commensals restore colonization resistance to Vancomycin-Resistant
449 *Enterococcus faecium*. Cell Host Microbe 21:592-602.e4.

450 5. Ubeda C, Bucci V, Caballero S, Djukovic A, Toussaint NC, Equinda M, Lipuma L, Ling L,
451 Gobourne A, No D, Taur Y, Jenq RR, van den Brink MR, Xavier JB, Pamer EG. 2013.
452 Intestinal microbiota containing *Barnesiella* species cures Vancomycin-Resistant
453 *Enterococcus faecium* colonization. Infect Immun 81:965–973.

454 6. Kim SG, Becattini S, Moody TU, Shliaha PV, Littmann ER, Seok R, Gjonbalaj M, Eaton V,
455 Fontana E, Amoretti L, Wright R, Caballero S, Wang Z-MX, Jung H-J, Morjaria SM, Leiner
456 IM, Qin W, Ramos RJJF, Cross JR, Narushima S, Honda K, Peled JU, Hendrickson RC, Taur
457 Y, Brink MRM van den, Pamer EG. 2019. Microbiota-derived lantibiotic restores resistance
458 against vancomycin-resistant *Enterococcus*. Nature 572:665–669.

459 7. Taur Y, Xavier JB, Lipuma L, Ubeda C, Goldberg J, Gobourne A, Lee YJ, Dubin KA, Socci
460 ND, Viale A, Perales M-A, Jenq RR, van den Brink MR, Pamer EG. 2012. Intestinal
461 domination and the risk of bacteremia in patients undergoing allogeneic hematopoietic stem
462 Cell Transplantation. Clin Infect Dis 55:905–914.

463 8. Hildebrand F, Moitinho-Silva L, Blasche S, Jahn MT, Gossmann TI, Huerta-Cepas J, Hercog
464 R, Luetge M, Bahram M, Pryszlak A, Alves RJ, Waszak SM, Zhu A, Ye L, Costea PI, Aalvink
465 S, Belzer C, Forslund SK, Sunagawa S, Hentschel U, Merten C, Patil KR, Benes V, Bork P.
466 2019. Antibiotics-induced monodominance of a novel gut bacterial order. Gut 68:1781.

467 9. Brandl K, Plitas G, Mihu CN, Ubeda C, Jia T, Fleisher M, Schnabl B, DeMatteo RP, Pamer
468 EG. 2008. Vancomycin-resistant enterococci exploit antibiotic-induced innate immune
469 deficits. Nature 455:804–807.

470 10. Mundt JO. 1963. Occurrence of enterococci in animals in a wild environment. Appl
471 Microbiol 11.

472 11. Stinear TP, Olden DC, Johnson PD, Davies JK, Grayson ML. 2001. Enterococcal vanB
473 resistance locus in anaerobic bacteria in human faeces. Lancet 357:855–856.

474 12. Lozupone C, Knight R. 2005. UniFrac: a new phylogenetic method for comparing
475 microbial communities. Appl Environ Microb 71:8228–8235.

476 13. Wang M, Carver JJ, Phelan VV, Sanchez LM, Garg N, Peng Y, Nguyen DD, Watrous J,
477 Kapono CA, Luzzatto-Knaan T, Porto C, Bouslimani A, Melnik AV, Meehan MJ, Liu W-T,
478 Crüsemann M, Boudreau PD, Esquenazi E, Sandoval-Calderón M, Kersten RD, Pace LA,
479 Quinn RA, Duncan KR, Hsu C-C, Floros DJ, Gavilan RG, Kleigrewe K, Northen T, Dutton
480 RJ, Parrot D, Carlson EE, Aigle B, Michelsen CF, Jelsbak L, Sohlenkamp C, Pevzner P, Edlund
481 A, McLean J, Piel J, Murphy BT, Gerwick L, Liaw C-C, Yang Y-L, Humpf H-U, Maansson
482 M, Keyzers RA, Sims AC, Johnson AR, Sidebottom AM, Sedio BE, Klitgaard A, Larson CB,
483 P CAB, Torres-Mendoza D, Gonzalez DJ, Silva DB, Marques LM, Demarque DP, Pociute E,
484 O'Neill EC, Briand E, Helfrich EJN, Granatosky EA, Glukhov E, Ryffel F, Houson H,
485 Mohimani H, Kharbush JJ, Zeng Y, Vorholt JA, Kurita KL, Charusanti P, McPhail KL, Nielsen
486 KF, Vuong L, Elfeki M, Traxler MF, Engene N, Koyama N, Vining OB, Baric R, Silva RR,
487 Mascuch SJ, Tomasi S, Jenkins S, Macherla V, Hoffman T, Agarwal V, Williams PG, Dai J,
488 Neupane R, Gurr J, Rodríguez AMC, Lamsa A, Zhang C, Dorrestein K, Duggan BM, Almaliti
489 J, Allard P-M, Phapale P, Nothias L-F, Alexandrov T, Litaudon M, Wolfender J-L, Kyle JE,
490 Metz TO, Peryea T, Nguyen D-T, VanLeer D, Shinn P, Jadhav A, Müller R, Waters KM, Shi
491 W, Liu X, Zhang L, Knight R, Jensen PR, Palsson BØ, Pogliano K, Linington RG, Gutiérrez
492 M, Lopes NP, Gerwick WH, Moore BS, Dorrestein PC, Bandeira N. 2016. Sharing and

493 community curation of mass spectrometry data with Global Natural Products Social Molecular
494 Networking. Nat Biotechnol 34:828–837.

495 14. Karki S, Houston L, Land G, Bass P, Kehoe R, Borrell S, Watson K, Spelman D, Kennon
496 J, Harrington G, Cheng AC. 2012. Prevalence and risk factors for VRE colonisation in a tertiary
497 hospital in Melbourne, Australia: a cross sectional study. Antimicrob Resist In 1:31.

498 15. Dubin K, Pamer EG. 2017. Enterococci and their interactions with the intestinal
499 microbiome. Microbiol Spectr 5.

500 16. Morton JT, Marotz C, Washburne A, Silverman J, Zaramela LS, Edlund A, Zengler K,
501 Knight R. 2019. Establishing microbial composition measurement standards with reference
502 frames. Nat Commun 10:2719.

503 17. Amir A, McDonald D, Navas-Molina JA, Kopylova E, Morton JT, Xu ZZ, Kightley EP,
504 Thompson LR, Hyde ER, Gonzalez A, Knight R. 2017. Deblur rapidly resolves single-
505 nucleotide community sequence patterns. mSystems 2:e00191-16.

506 18. Morrison DJ, Preston T. 2016. Formation of short chain fatty acids by the gut microbiota
507 and their impact on human metabolism. Gut Microbes 7:189–200.

508 19. Dubin KA, Mathur D, McKenney PT, Taylor BP, Littmann ER, Peled JU, van den Brink
509 MR, Taur Y, Pamer EG, Xavier JB. 2019. Diversification and evolution of vancomycin-
510 resistant *Enterococcus faecium* during intestinal domination. Infect Immun 87.

511 20. Buffie CG, Pamer EG. 2013. Microbiota-mediated colonization resistance against intestinal
512 pathogens. Nat Rev Immunol 13:790–801.

513 21. Sorbara MT, Dubin K, Littmann ER, Moody TU, Fontana E, Seok R, Leiner IM, Taur Y,
514 Peled JU, Brink MRM van den, Litvak Y, Bäumler AJ, Chaubard J-L, Pickard AJ, Cross JR,
515 Pamer EG. 2018. Inhibiting antibiotic-resistant Enterobacteriaceae by microbiota-mediated
516 intracellular acidification. J Exp Medicine 216:84–98.

517 22. Lawhon SD, Maurer R, Suyemoto M, Altier C. 2002. Intestinal short-chain fatty acids alter
518 *Salmonella typhimurium* invasion gene expression and virulence through BarA/SirA. Mol
519 Microbiol 46:1451–1464.

520 23. Gantois I, Ducatelle R, Pasmans F, Haesebrouck F, Hautefort I, Thompson A, Hinton JC,
521 Immerseel FV. 2006. Butyrate specifically down-regulates *Salmonella* pathogenicity island 1
522 gene expression. Appl Environ Microb 72:946–949.

523 24. Thompson LR, Sanders JG, McDonald D, Amir A, Ladau J, Locey KJ, Prill RJ, Tripathi
524 A, Gibbons SM, Ackermann G, Navas-Molina JA, Janssen S, Kopylova E, Vázquez-Baeza Y,
525 González A, Morton JT, Mirarab S, Xu ZZ, Jiang L, Haroon MF, Kanbar J, Zhu Q, Song SJ,
526 Kosciolek T, Bokulich NA, Lefler J, Brislawn CJ, Humphrey G, Owens SM, Hampton-Marcell
527 J, Berg-Lyons D, McKenzie V, Fierer N, Fuhrman JA, Clauset A, Stevens RL, Shade A,
528 Pollard KS, Goodwin KD, Jansson JK, Gilbert JA, Knight R, Rivera JLA, Al-Moosawi L,
529 Alverdy J, Amato KR, Andras J, Angenent LT, Antonopoulos DA, Apprill A, Armitage D,
530 Ballantine K, Bárta J, Baum JK, Berry A, Bhatnagar A, Bhatnagar M, Biddle JF, Bittner L,
531 Boldgiv B, Bottos E, Boyer DM, Braun J, Brazelton W, Brearley FQ, Campbell AH, Caporaso
532 JG, Cardona C, Carroll J, Cary SC, Casper BB, Charles TC, Chu H, Claar DC, Clark RG,
533 Clayton JB, Clemente JC, Cochran A, Coleman ML, Collins G, Colwell RR, Contreras M,
534 Crary BB, Creer S, Cristol DA, Crump BC, Cui D, Daly SE, Davalos L, Dawson RD, Defazio
535 J, Delsuc F, Dionisi HM, Dominguez-Bello MG, Dowell R, Dubinsky EA, Dunn PO, Ercolini
536 D, Espinoza RE, Ezenwa V, Fenner N, Findlay HS, Fleming ID, Fogliano V, Forsman A,

537 Freeman C, Friedman ES, Galindo G, Garcia L, Garcia-Amado MA, Garshelis D, Gasser RB,
538 Gerdts G, Gibson MK, Gifford I, Gill RT, Giray T, Gittel A, Golyshin P, Gong D, Grossart H-
539 P, Guyton K, Haig S-J, Hale V, Hall RS, Hallam SJ, Handley KM, Hasan NA, Haydon SR,
540 Hickman JE, Hidalgo G, Hofmockel KS, Hooker J, Hulth S, Hultman J, Hyde E, Ibáñez-Álamo
541 JD, Jastrow JD, Jex AR, Johnson LS, Johnston ER, Joseph S, Jurburg SD, Jurelevicius D,
542 Karlsson A, Karlsson R, Kauppinen S, Kellogg CTE, Kennedy SJ, Kerkhof LJ, King GM,
543 Kling GW, Koehler AV, Krezalek M, Kueneman J, Lamendella R, Landon EM, Lane-deGraaf
544 K, LaRoche J, Larsen P, Laverock B, Lax S, Lentino M, Levin II, Liancourt P, Liang W, Linz
545 AM, Lipson DA, Liu Y, Lladser ME, Lozada M, Spirito CM, MacCormack WP, MacRae-
546 Crerar A, Magris M, Martín-Platero AM, Martín-Vivaldi M, Martínez LM, Martínez-Bueno
547 M, Marzinelli EM, Mason OU, Mayer GD, McDevitt-Irwin JM, McDonald JE, McGuire KL,
548 McMahon KD, McMinds R, Medina M, Mendelson JR, Metcalf JL, Meyer F, Michelangeli F,
549 Miller K, Mills DA, Minich J, Mocali S, Moitinho-Silva L, Moore A, Morgan-Kiss RM,
550 Munroe P, Myrold D, Neufeld JD, Ni Y, Nicol GW, Nielsen S, Nissimov JI, Niu K, Nolan MJ,
551 Noyce K, O'Brien SL, Okamoto N, Orlando L, Castellano YO, Osuolale O, Oswald W, Parnell
552 J, Peralta-Sánchez JM, Petraitis P, Pfister C, Pilon-Smits E, Piombino P, Pointing SB, Pollock
553 FJ, Potter C, Prithiviraj B, Quince C, Rani A, Ranjan R, Rao S, Rees AP, Richardson M,
554 Riebesell U, Robinson C, Rockne KJ, Rodriguezl SM, Rohwer F, Roundstone W, Safran RJ,
555 Sangwan N, Sanz V, Schrenk M, Schrenzel MD, Scott NM, Seger RL, Seguin-Orlando A,
556 Seldin L, Seyler LM, Shakhsheer B, Sheets GM, Shen C, Shi Y, Shin H, Shogan BD, Shutler
557 D, Siegel J, Simmons S, Sjöling S, Smith DP, Soler JJ, Sperling M, Steinberg PD, Stephens B,
558 Stevens MA, Taghavi S, Tai V, Tait K, Tan CL, Tas¸ N, Taylor DL, Thomas T, Timling I,
559 Turner BL, Urich T, Ursell LK, Lelie D van der, Treuren WV, Zwieten L van, Vargas-Robles
560 D, Thurber RV, Vitaglione P, Walker DA, Walters WA, Wang S, Wang T, Weaver T, Webster
561 NS, Wehrle B, Weisenhorn P, Weiss S, Werner JJ, West K, Whitehead A, Whitehead SR,

562 Whittingham LA, Willerslev E, Williams AE, Wood SA, Woodhams DC, Yang Y, Zaneveld
563 J, Zarraonaindia I, Zhang Q, Zhao H. 2017. A communal catalogue reveals Earth's multiscale
564 microbial diversity. Nature 551:457–463.

565 25. Gonzalez A, Navas-Molina JA, Kosciolek T, McDonald D, Vázquez-Baeza Y, Ackermann
566 G, DeReus J, Janssen S, Swafford AD, Orchanian SB, Sanders JG, Shorenstein J, Holste H,
567 Petrus S, Robbins-Pianka A, Brislawn CJ, Wang M, Rideout JR, Bolyen E, Dillon M, Caporaso
568 JG, Dorrestein PC, Knight R. 2018. Qiita: rapid, web-enabled microbiome meta-analysis. Nat
569 Methods 15:796–798.

570 26. Bolyen E, Rideout JR, Dillon MR, Bokulich NA, Abnet CC, Al-Ghalith GA, Alexander H,
571 Alm EJ, Arumugam M, Asnicar F, Bai Y, Bisanz JE, Bittinger K, Brejnrod A, Brislawn CJ,
572 Brown CT, Callahan BJ, Caraballo-Rodríguez AM, Chase J, Cope EK, Silva RD, Diener C,
573 Dorrestein PC, Douglas GM, Durall DM, Duvallet C, Edwardson CF, Ernst M, Estaki M,
574 Fouquier J, Gauglitz JM, Gibbons SM, Gibson DL, Gonzalez A, Gorlick K, Guo J, Hillmann
575 B, Holmes S, Holste H, Huttenhower C, Huttley GA, Janssen S, Jarmusch AK, Jiang L, Kaehler
576 BD, Kang KB, Keefe CR, Keim P, Kelley ST, Knights D, Koester I, Kosciolek T, Kreps J,
577 Langille MGI, Lee J, Ley R, Liu Y-X, Loftfield E, Lozupone C, Maher M, Marotz C, Martin
578 BD, McDonald D, McIver LJ, Melnik AV, Metcalf JL, Morgan SC, Morton JT, Naimey AT,
579 Navas-Molina JA, Nothias LF, Orchanian SB, Pearson T, Peoples SL, Petras D, Preuss ML,
580 Pruesse E, Rasmussen LB, Rivers A, Robeson MS, Rosenthal P, Segata N, Shaffer M, Shiffer
581 A, Sinha R, Song SJ, Spear JR, Swafford AD, Thompson LR, Torres PJ, Trinh P, Tripathi A,
582 Turnbaugh PJ, Ul-Hasan S, Hooft JJJ van der, Vargas F, Vázquez-Baeza Y, Vogtmann E,
583 Hippel M von, Walters W, Wan Y, Wang M, Warren J, Weber KC, Williamson CHD, Willis
584 AD, Xu ZZ, Zaneveld JR, Zhang Y, Zhu Q, Knight R, Caporaso JG. 2019. Reproducible,

585 interactive, scalable and extensible microbiome data science using QIIME 2. Nat Biotechnol
586 37:852–857.

587 27. Pedregosa F, Varoquaux G, Gramfort A, Michel V, Thirion B, Grisel O, Blondel M, Müller
588 A, Nothman J, Louppe G, Prettenhofer P, Weiss R, Dubourg V, Vanderplas J, Passos A,
589 Cournapeau D, Brucher M, Perrot M, Duchesnay É. 2012. Scikit-learn: machine learning in
590 python.

591 28. Janssen S, McDonald D, Gonzalez A, Navas-Molina JA, Jiang L, Xu ZZ, Winker K, Kado
592 DM, Orwoll E, Manary M, Mirarab S, Knight R. 2018. Phylogenetic placement of exact
593 amplicon sequences improves associations with clinical information. mSystems 3:e00021-18.

594 29. Masukagami Y, Nijagal B, Mahdizadeh S, Tseng C-W, Dayalan S, Tivendale KA,
595 Markham PF, Browning GF, Sansom FM. 2019. A combined metabolomic and bioinformatic
596 approach to investigate the function of transport proteins of the important pathogen
597 *Mycoplasma bovis*. Vet Microbiol 234:8–16.

598 30. Pluskal T, Castillo S, Villar-Briones A, Orešič M. 2010. MZmine 2: Modular framework
599 for processing, visualizing, and analyzing mass spectrometry-based molecular profile data.
600 BMC Bioinformatics 11:395.

601 31. Morton JT, Aksenov AA, Nothias LF, Foulds JR, Quinn RA, Badri MH, Swenson TL,
602 Goethem MWV, Northen TR, Vazquez-Baeza Y, Wang M, Bokulich NA, Watters A, Song SJ,
603 Bonneau R, Dorrestein PC, Knight R. 2019. Learning representations of microbe–metabolite
604 interactions. Nat Methods 1–9.

605

Day of experiment	0	1	2	3	4	5	6	7	8	9	10	11	12	13	14
Phase of experiment*	N	N	N	N	N	N	Abx-Tx	Abx-Tx	Abx-Wn	VRE-E	VRE-E	VRE-E	VRE-E	VRE-L	VRE-L
Amplicon 16S rRNA gene data	✓	✓	✓	-	-	✓	✓	✓	✓	✓	-	-	✓	✓	✓
Metabolomics	✓	-	-	-	-	✓	✓	✓	✓	✓	-	-	-	-	✓
Avg observed sOTUs#	210	220	220	-	-	225	112	84	93	30	-	-	22	34	53

Table 1: Summary of samples analyzed in this study

Notes: *The key phases of the experiment where, N represents Naïve; Abx-Tx represents Antibiotic treatment; Abx-Wn represents Antibiotic weaning; VRE-E represents Early-phase post-VREfm colonisation; and VRE-L represents Late-phase post-VREfm colonization; #The average number of sOTUs observed across all mice for each day of the experiment; '✓' Sample processed; '-' Data unavailable

613 **Figures**

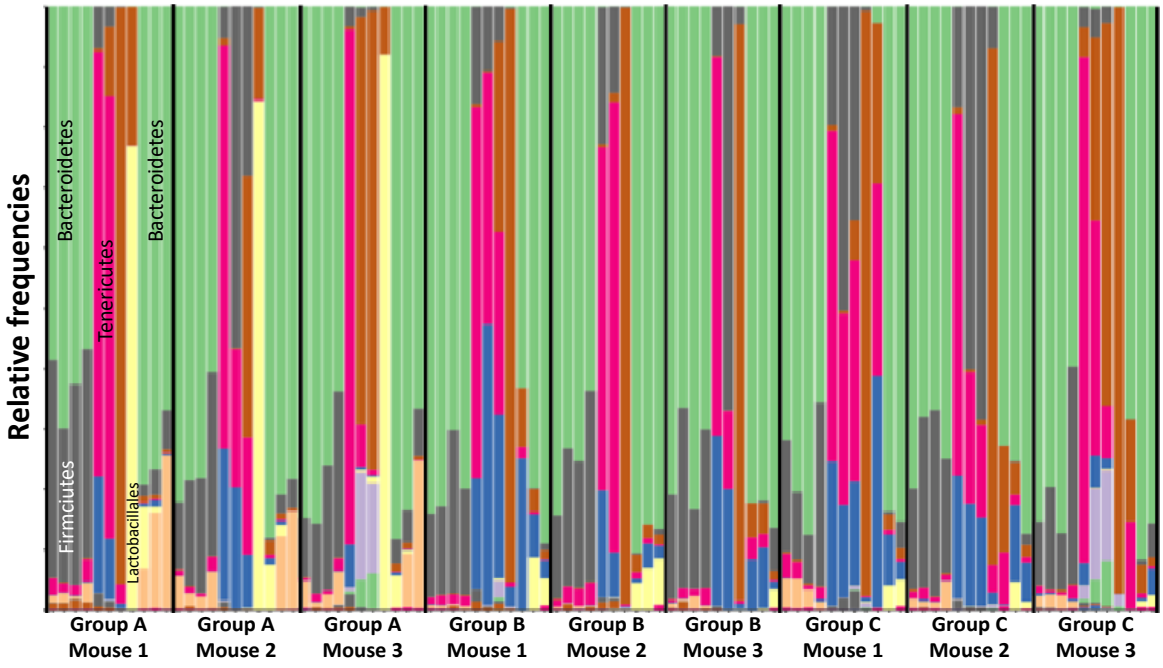

614

615 **Figure 1 Biodiversity plot of sOTUs as relative frequencies at the taxonomic level of Class.**
616 First-order shifts in microbial community composition, as revealed by 16S rRNA gene
617 community profiling, from a predominance of Bacteroidetes to Tenericutes and return to
618 Bacteroidetes was observed. Each column displays the relative bacterial community
619 composition in a mouse faecal sample collected daily and sorted by the chronology of the
620 experiment (i.e., Day of experiment; Table 1). The columns are further sorted by group (i.e.,
621 Group A, Group B, and Group C) and individual mice within each group (mouse 1, mouse 2,
622 and mouse 3). Stacked bars are presented as relative frequencies at the taxonomical level of
623 Class, however, annotations of key taxa are at the phyla level (Bacteroidetes, green; Firmicutes,
624 grey; and Tenericutes, fuschia) or Order level (Lactobacillales, yellow).

625

626

627

628

629

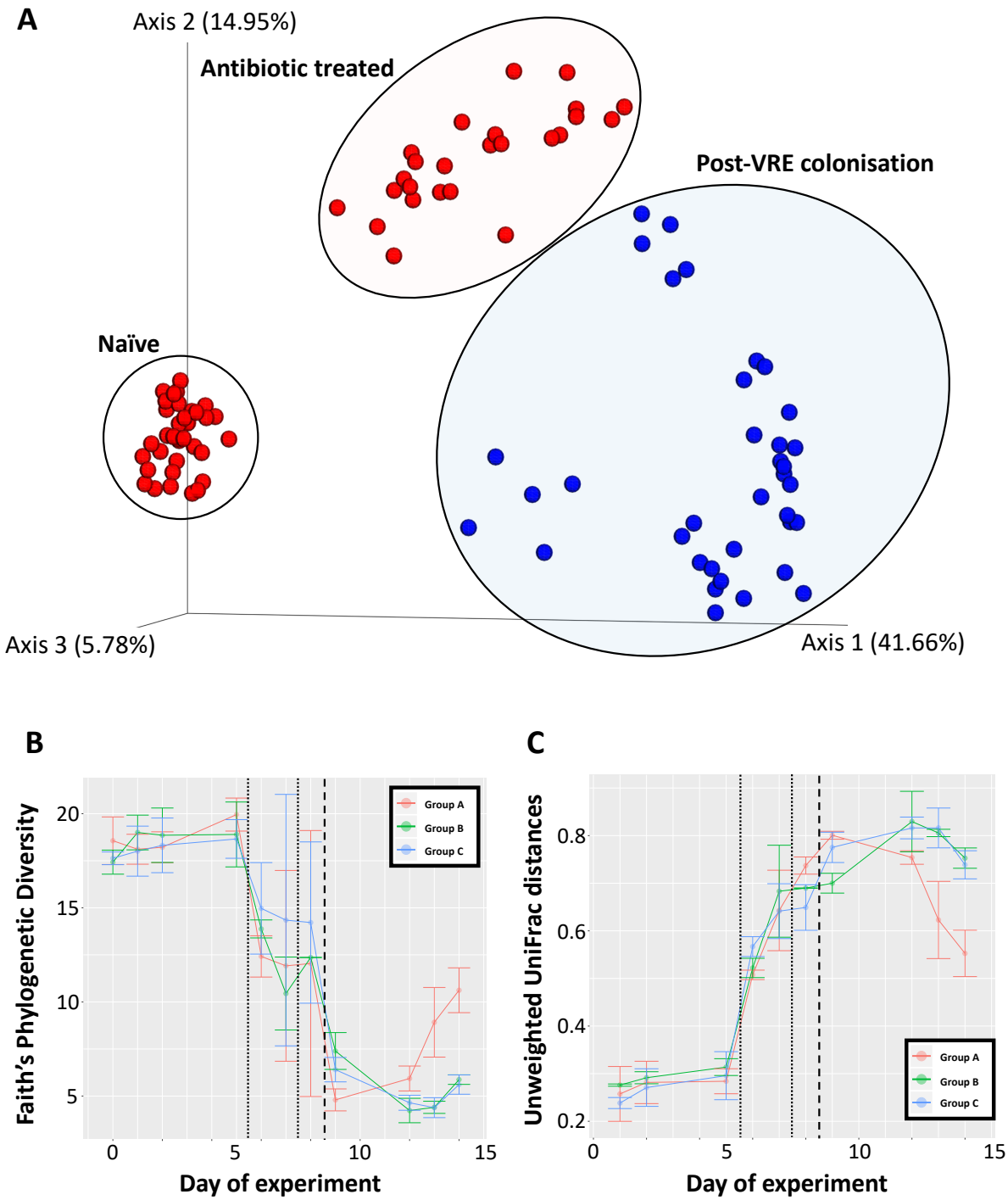

Figure 2 Diversity analyses. (A) Principal coordinate analysis plot of unweighted UniFrac distances. Data points are projected onto the sample space, and coloured by pre-VREfm colonisation (red), and post-VREfm colonisation (blue). *n.b.,* circles and ellipses function to highlight the separation of experimental phases and do not indicate statistical confidence intervals. Principal coordinate axis 1 explains 41.66% of the variation observed between the

636 naïve microbiota and those from the post-VREfm colonisation phase. **(B)** Community richness
637 of the murine gut microbiome, as measured by Faith's Phylogenetic Diversity, in response to
638 ceftriaxone treatment and challenge with VREfm; **(C)** community dissimilarity distances, as
639 calculated by unweighted UniFrac, of each time point relative to day 0 (naïve phase).
640

Positively associated with colonisation	
Enterococcus	1.6693
Bacteroides	1.0559
Erysipelotrichaceae	1.0521
Catabacter	0.8159
Lachnospiraceae	0.7848
Negative association with colonisation	
Clostridiales	-4.0947
Adlercreutzia	-3.8292
Mollicutes	-3.8392
Peptostreptococcaceae	-3.7357
Clostridiales	-3.5084

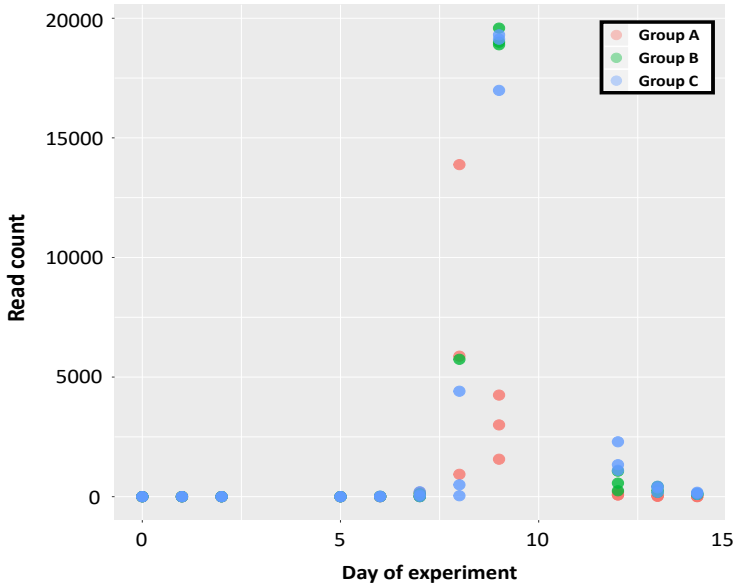

641

642 **Figure 3 Multinomial regression.** Multinomial regression identified an *Enterococci* exact
643 sequence variant as the most positively associated with the colonisation phase (log-fold change
644 score of 1.6693). Read counts for the *Enterococci*-ESV tracked daily across the experiment
645 showing high abundance during days of VREfm challenge.

646

647

648

649

650

651

652

653

654

655

656

657

658

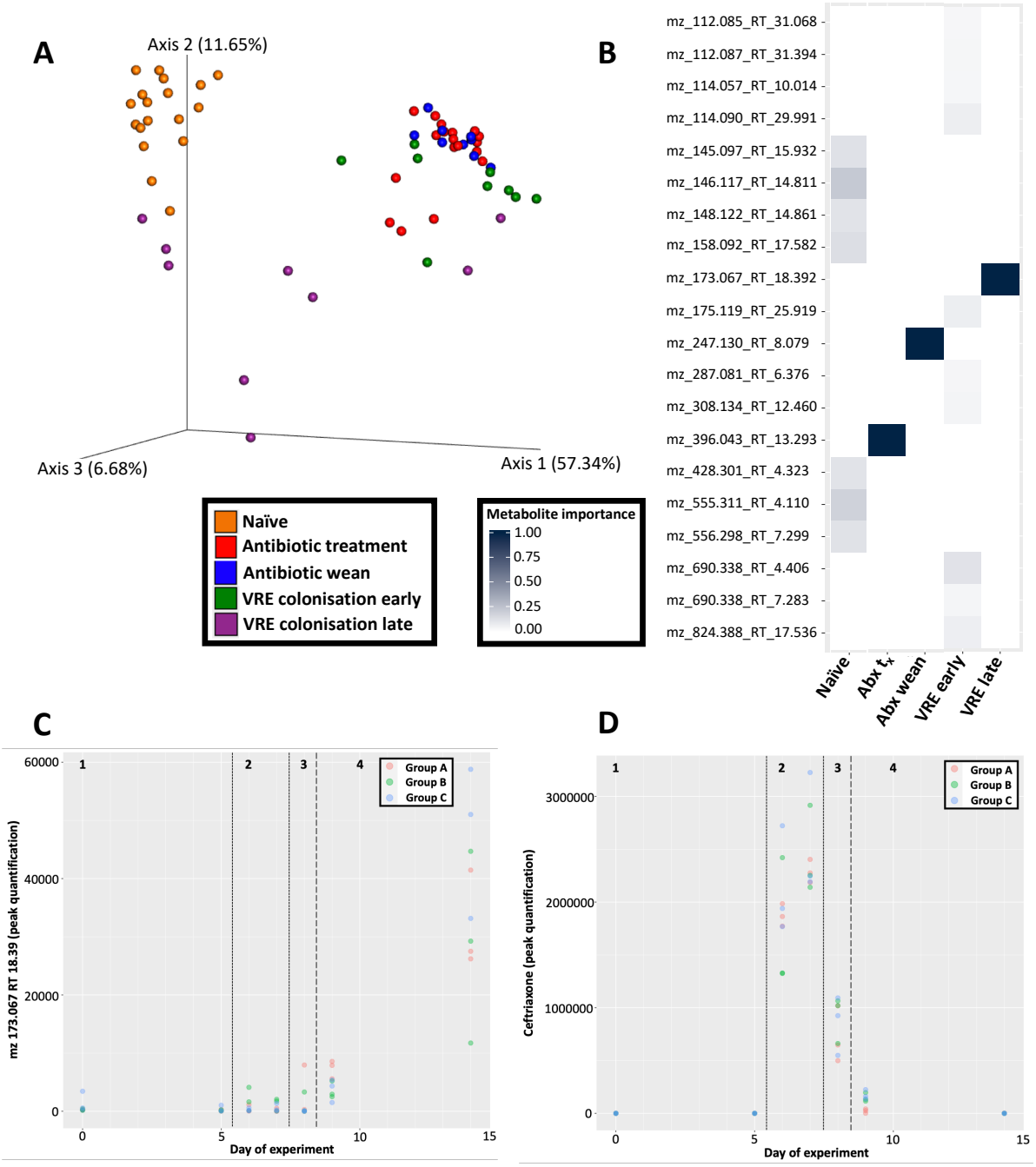

Figure 4 Metabolomic analyses. (A) Emperor plot displaying principal coordinate analysis of binary Jaccard distances of metabolomic profiles. Samples represent (colour coded) the naïve (orange), antibiotic-treatment (red), antibiotic-weaning (blue), early-VRE colonisation (green), and late-VREfm colonisation (purple) phases. **(B)** Random Forest classifier identifying metabolite features (spectra) for each phase of the experiment. Heatmap is colour-coded from low ranking score (white; i.e., lowest importance) to high ranking score (dark blue; highest

importance). Metabolite features are labelled by their mass-charge ratios and retention times for the reason that current databases do not capture their chemical structure and/or identifications. **(C)** Peak quantification values for feature 6325 (m/z= 172.0671 RT = 18.39) present in abundance during *VRE colonisation late* (phase 4). **(D)** Peak quantification values for ceftriaxone (m/z = 555.0537 RT = 13.30) tracked across the experiment. Ceftriaxone values are highest during *antibiotic treatment* (phase 2) and begins to wane during *antibiotic wean* (phase 3).

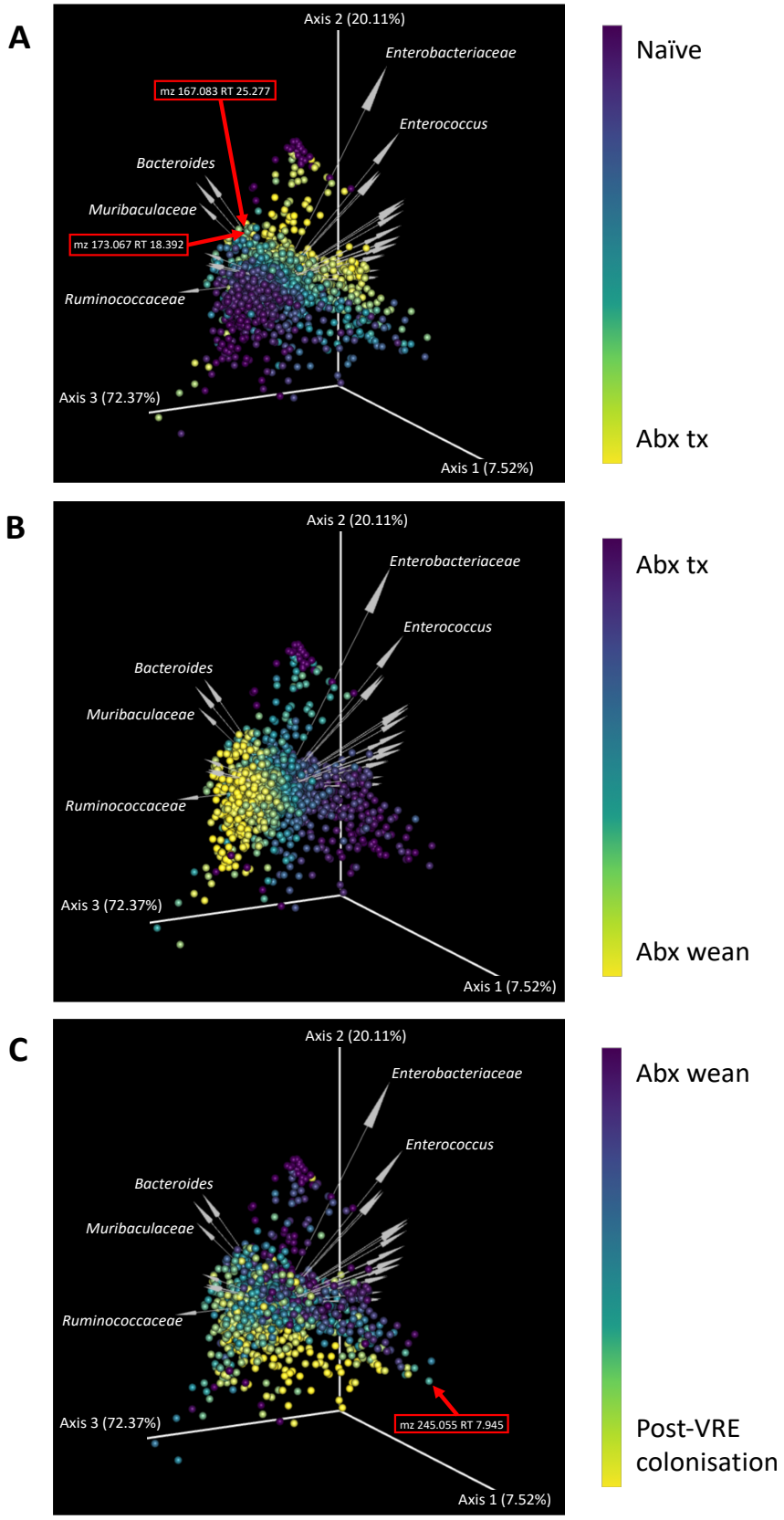

691

692 **Figure 5 Microbe-metabolite vector biplots.** Sequential biplots highlighting the changing

693 metabolite differentials across each key phase of the experiment; where *abx tx* corresponds to

694 the *antibiotic treatment* phase, and *abx wean* corresponds to the period where antibiotics were
695 removed for a 24-hour period prior to colonisation with VREfm. Each point on the sample
696 space represents metabolites, and arrows represent microbes. Microbe and metabolite features
697 are fixed upon the sample space, with gradient coloring of metabolites indicating the transition
698 across key phases of the experiment. The distance between each point is indicative of
699 metabolite co-occurrence frequency, and the angle between arrows indicate microbial co-
700 occurrence. The directionality of the arrows describes the variation in the metabolites explained
701 the microbes represented by the arrows. For example, metabolite feature 6325 (m/z 173.067
702 RT 18.392) is demonstrated to co-occur with *Bacteroides*. Information about the abundances
703 of these co-occurring features are provided as heatmaps in Supplementary Figure 6.
704
705

706 **Supplementary figures**

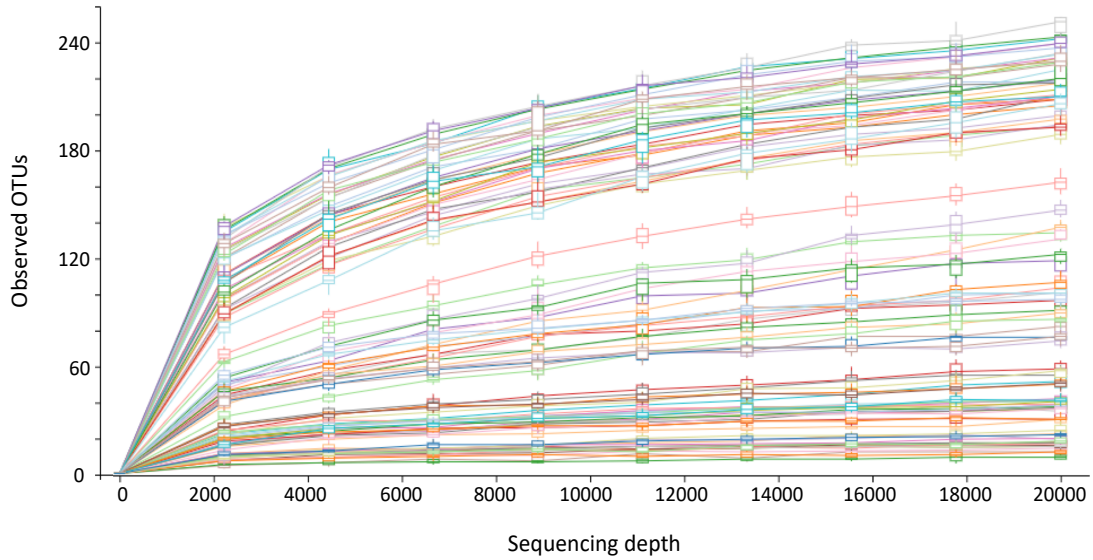

707

708 **Supplementary Figure 1** Alpha rarefaction plot of all samples rarefied to 20,000 reads per

709 sample.

710

711

712

713

714

715

716

717

718

719

720

721

722

723

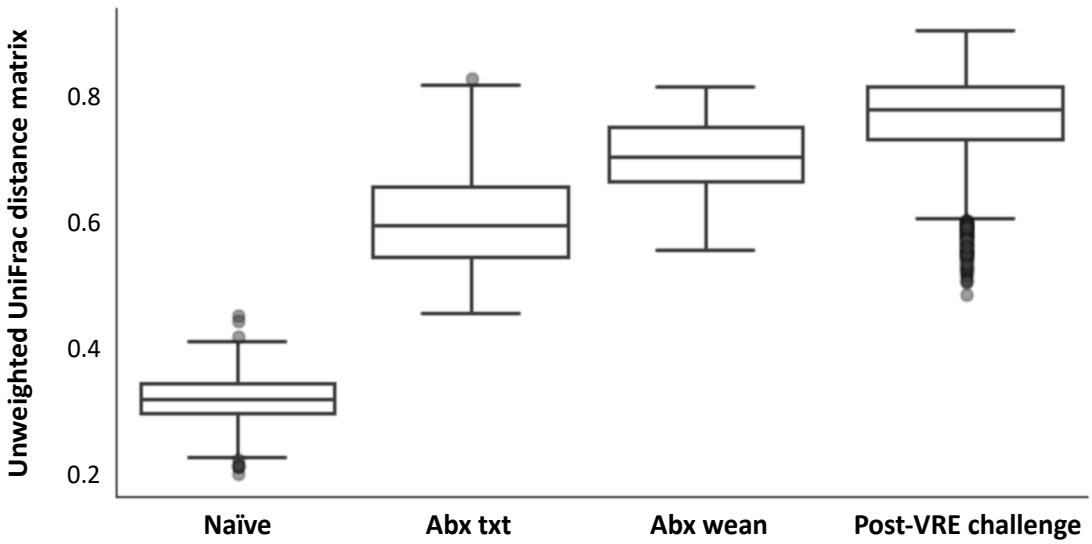

Supplementary Figure 2 PERMANOVA testing (999 permutations) on unweighted UniFrac distances (16S rRNA gene data) relative to samples from the naïve phase. P-values for pairwise PERMANOVA testing given in parentheses for the following phases of the experiment: naïve – antibiotic treatment (0.001); naïve – antibiotic treatment (0.001); naïve – infection (0.001); antibiotic treatment – antibiotic wean (0.025).

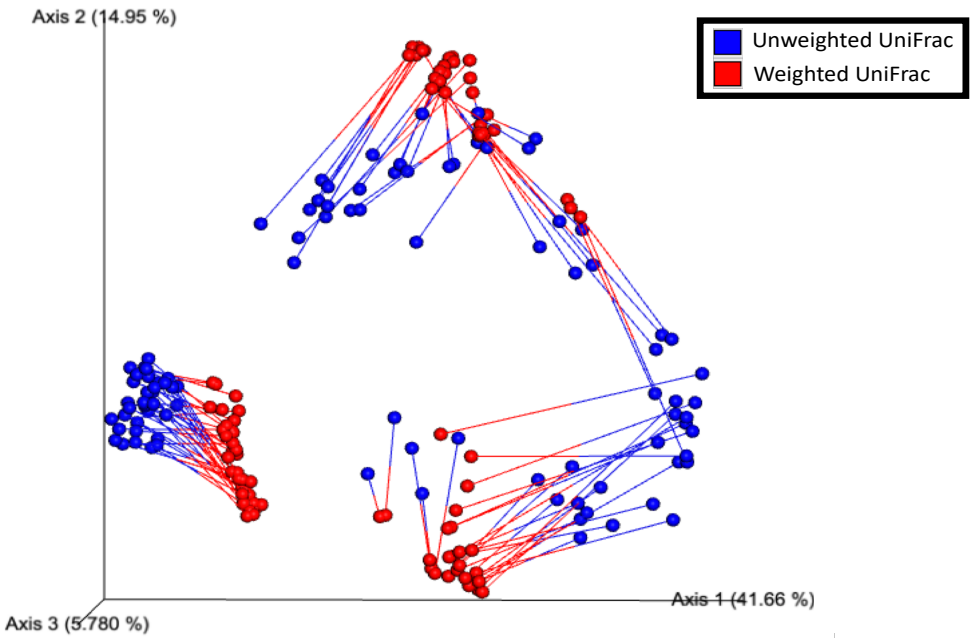

Supplementary Figure 3 Emperor plot of procrustes analysis of unweighted (blue) and weighted (red) UniFrac distance metrices.

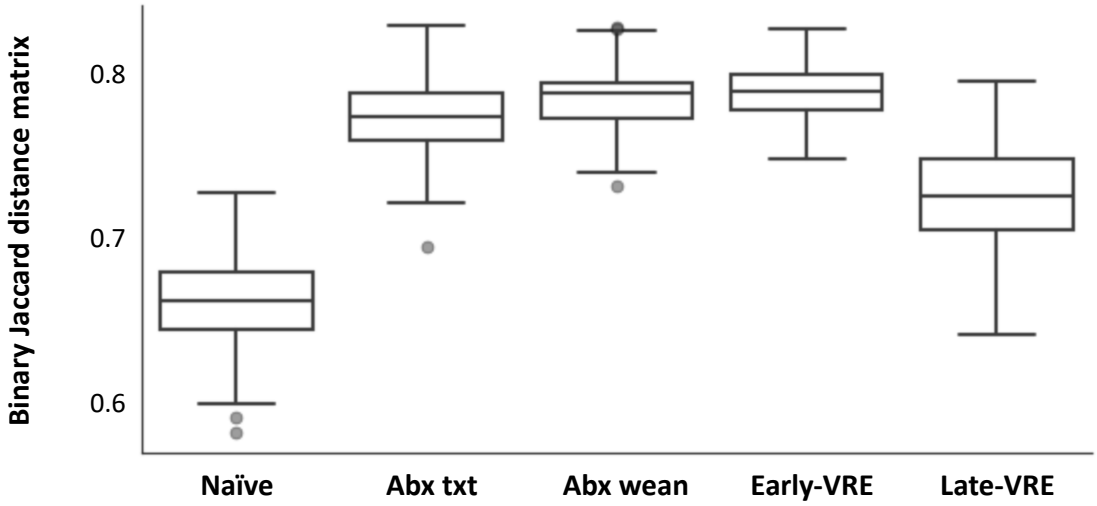

759

760 **Supplementary Figure 4** Pairwise PERMANOVA testing (999 permutations) on binary
761 Jaccard distances (metabolome data) relative to samples from the naïve phase. While naïve and
762 late-VRE samples are significantly different, late-VRE has a lower distance to naïve compared
763 to Abx txt, Abx wean and early-VRE samples.

764

765

766

767

768

769

770

771

772

773

774

775

776

777

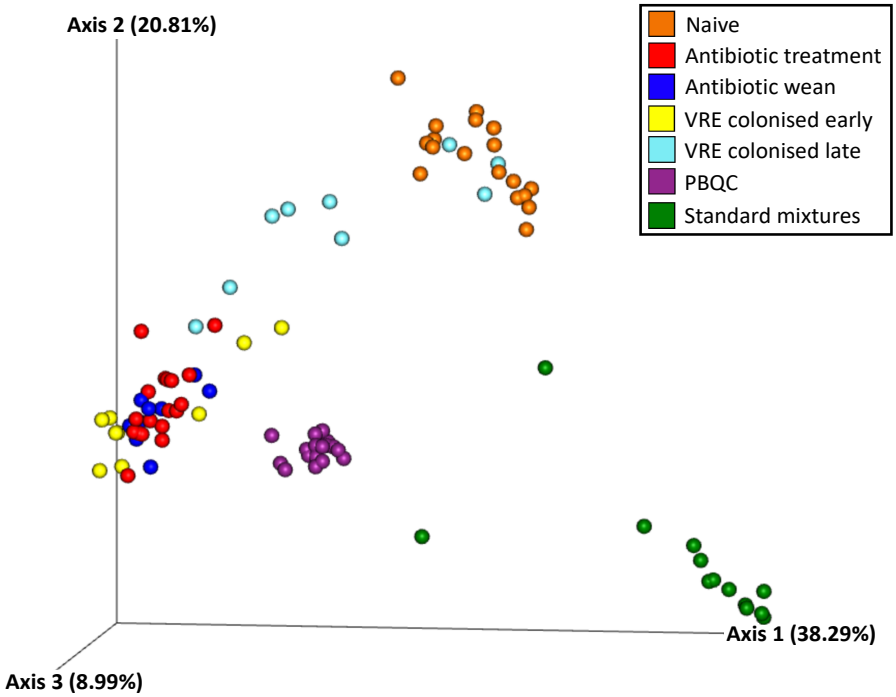

Supplementary Figure 5 Emperor visualization displaying samples assayed for metabolomics. Principal coordinate analysis plot of distances between each sample based on their overlapping molecules as measured by Binary Jaccard. Samples assayed include pooled biological quality control samples (purple), and samples of known standard metabolite mixtures (green). The general metabolome profile of test samples is retained.

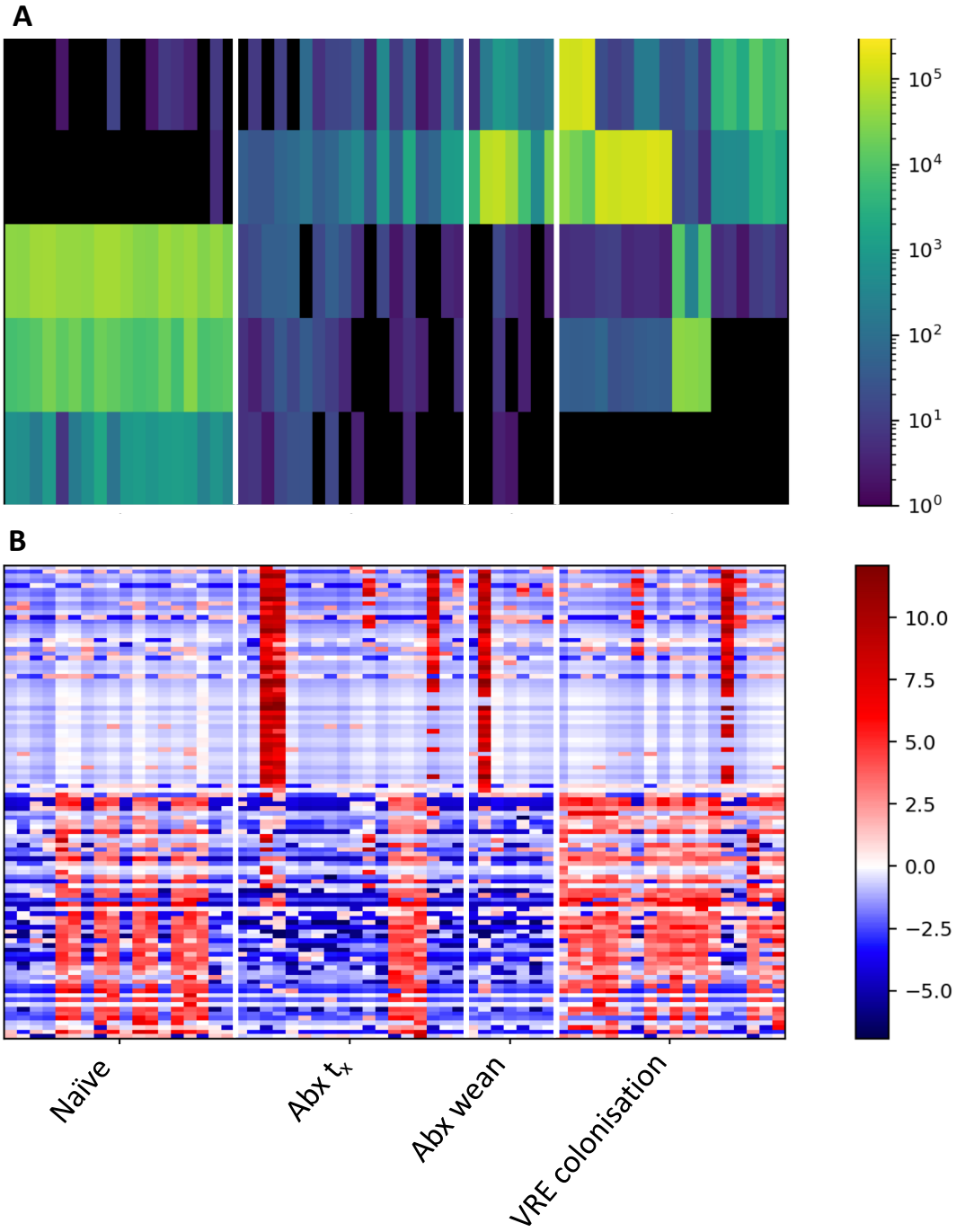

794

795 **Supplementary Figure 6 Paired feature abundance heatmaps. (A)** Microbe abundances
796 and **(B)** metabolite log centered abundances across each phase of the experiment. Heatmaps
797 are aligned along the x-axis (phase of experiment); y-axis displays microbe and metabolite
798 abundances.

799